Applied Ocean Research 115 (2021) 102827

Contents lists available at ScienceDirect

Applied Ocean Research

journal homepage: www.elsevier.com/locate/apor

# Investigating the winch performance in an ASV/ROV autonomous inspection system

Chenyu Zhao [a], Philipp R. Thies [a,*], Lars Johanning [a,b]

[a] Renewable Energy Group, College of Engineering, Mathematics and Physical Sciences, University of Exeter, UK
[b] Naval Architecture, Harbin Engineering University, Nantong Main Street 145, Nangang District, Harbin, China

ARTICLE INFO

*Keywords:*
Autonomous systems
ROV
ASV
Winch system
Analytical and numerical approaching
Control

ABSTRACT

Combined Autonomous Surface Vehicles (ASV) and remotely operated underwater vehicles (ROV) inspection and intervention systems can contribute to future asset management of offshore renewable energy. This paper presents the design and performance of the winch system which couples the ASV and ROV and deploys/recovers the ROV. The hydrodynamic models and control algorithms are developed and solved with analytical and numerical approaches. The winch performance needs to meet a range of operational profiles, including i) ASV following/not following the ROV ii) winch operating in speed control iii) winch operating in tension control iv) varying ROV distance and depths targets. For a representative ASV/ROV configuration, the work determines the required umbilical length for different ROV targets and suitable winch speeds. The results show that the strategy where the ASV follows the ROV can reduce the umbilical tension, but conditions of compression should be carefully managed. The umbilical tension can also be decreased by tension control and shows to be very effective in larger sea states. This study also models the accidental limit case, where a malfunctioning ROV is recovered. The estimated increase of umbilical tension during the recovery stage of a malfunctioning ROV can thus be incorporated into the design calculations.

## Introduction

With increasing offshore renewable installations, currently driven through offshore wind installations, the need for subsea interventions continues to rise worldwide (DeCastro et al., 2019, Lian et al., 2019). Offshore wind farms require inspections to comply with statutory regulations, asset management and condition monitoring purposes (Chung et al., 2020). These inspections' subsea element commonly involves the wind turbine foundations and submarine cables (Jin et al., 2019).

Increased autonomy of inspection and maintenance operations has well-recognised advantages in reducing the exposure of humans offshore. The G+ Global Offshore Wind Health and Safety Organisation monitors and reports incident data. Their 2019 incident data report Organisation Ghas (2019) listed 865 health and safety incidents, of which 245 occurred on vessels. A third of 252 high potential incidents, defined as incidents having the potential to cause fatalities, occurred on Crew Transfer Vessels. Thus, autonomous intervention systems present the opportunity to gradually reduce this risk, in particular for far offshore farms with over 100km distance-to-shore.

A medium-term 10-15year vision in the offshore sector is "(…) that routine inspection and maintenance tasks on offshore wind farms will be mostly conducted by autonomous platforms working with human operators located onshore." Hill (2019) The autonomous systems have to be modelled, demonstrated, and trialled to realise this ambition before they can be routinely deployed for operational offshore asset management. This paper introduces the topic with a brief review of the system components, namely ROV, ASV and winch, and the recent developments in coupled system modelling.

ROVs are classified as inspection-class and intervention-class vehicles based on their task requirements and rated working depth (Capocci et al., 2017). The intervention-class device is normally bulky (200 kg to 5,000 kg) and robust so that it can operate in deep water (up to 10,000 m) but are extremely high cost. For example, the "KAIKO" was constructed by Japan in 1995. The sea trial results demonstrated that its maximum operating depth could reach 10,000 m (Kyo et al., 1995, Mikagawa and Fukui, 1999). After KAIKO, more 10,000 m-class ROVs were promoted such as "ASSS-11k" (Ishibashi et al., 2007) and "UROV-11k" (Nakajoh et al., 2018), both of which have an 11,000 m depth capacity.

The inspection-class ROV has a smaller mass and lower cost (Capocci et al., 2017) and is more suitable for offshore renewable energy (ORE), operating in relatively shallow water, less than 300 m. Recent examples

* Corresponding author.

https://doi.org/10.1016/j.apor.2021.102827
Received 30 March 2021; Received in revised form 27 July 2021; Accepted 1 August 2021
Available online 17 August 2021

include the modelling of an ROV deployment to inspect the OC3-Hywind floating wind turbine in (Bruno et al., 2015). Sivčev, Omerdić (Sivčev et al., 2017) presented a long-term inspection ROV with Smart Tether Management System (STMS), which is designed for floating wind farms. The conceptual design and hydrodynamic performance of ROV inspection and monitoring for marine renewable energy projects is also considered in (Rush et al., 2014, Joslin et al., 2014). The inspection -ROV has also been studied for a range of other shallow-water structures, like dam, breakwaters (Sun Y-s et al., 2012, Cruz et al., 2011, Chen et al., 2015, Yu et al., 2021) and ship hull inspection (Negahdaripour and Firoozfam, 2006).

In the last ten years, the rapid development of control methods and AI techniques allow more inspection-ROVs to be supported by an Autonomous Surface Vehicles (ASV) (Matsuda et al., 2020, Chen et al., 2021). This integration enables a fully autonomous inspection system (Zhao et al., 2020, Gray and Schwartz, 2016). Recent successful sea trials have demonstrated that the ASV/ROV system has a significant advantage (such as low human risk and more flexible payload) compared to the traditional crewed system, especially in a potential hash sea environment (Conte et al., 2017, Conte et al., 2016). However, the ASV/ROV system is also facing some new challenges, one of which is the winch system design. In an ASV/ROV system, the ROV is connected to the ASV by a winch which is the main component of the launch and recovery system (LARS) (Sarda and Dhanak, 2016). The coupled effects caused by the LARS operations will significantly influence the tension on the umbilical (Zhao et al., 2020, Sivčev et al., 2018). The traditional towing winch used in the offshore structure or the ship usually has a large tension capacity, as well as a large mass, which is not suitable for the lighter and smaller ASV vessels. Some potential winch solutions include the cage-type TMS with an ROV compensating the heave motion to stable the umbilical tension and enhance the environment capacity of the whole system (Trslic et al., 2020). The digital hydraulic winch also showed potential in the ASV/ROV system owing to its high response speed and efficiency (Nordås et al., 2017).

This study aims to evaluate the performance in an ASV/ROV system through a fully coupled hydrodynamic model. The winch speed control and winch tension control are the most common (Pardo et al., 2017) strategies and are both modelled. In the speed control, the winch will pay out or haul in at a constant speed. If operated under tension control, the winch speed is changeable to maintain the umbilical tension close to the set point. In addition, a motion compensate system was modelled under tension control to mitigate sudden relative speed changes, and the resulting umbilical peak tensions, between ASV and ROV. The ASV in this paper used two control strategies to represent different realistic operational scenarios: holding the position target and following the ROV. The remainder of the paper is organised as follows: Section 2 lays out the analytical model of the ASV, ROV and winch with control methods. Section 3 presents the numerical modelling of the ASV/ROV system, including the cases and numerical tools. The tension performance results of winch/umbilical are introduced in Section 4. Section 5 discusses the main findings in light of potential industrial applications and further R&D requirements. Section 6 concludes with the main findings and outcomes.

## Analytical modelling

The analytical hydrodynamic methods to model the coupled ASV/ROV system have been established in previous studies (Fossen, 1999, Feng and Allen, 2004). The methods have been implemented, applied and partly validated for a coupled ASV/ROV system in (Zhao et al., 2020),which described the detailed hydrodynamic model setup. This section and the focus of the current paper lies in the control function and strategy of the ASV, the ROV and the winch system. The coordinate systems and dynamic equation of umbilical are also listed in the appendix to help readers to recall.

### *The ASV control*

The control force matrix of the non-following ASV is designed to hold the vessel position but with a small drifting, which is presented as:

$$[C]=\begin{bmatrix} C_1(x_{ASV}-x_0) & 0 & 0 & 0 & 0 & 0 \\ 0 & C_2(y_{ASV}-y_0) & 0 & 0 & 0 & 0 \\ 0 & 0 & 0 & 0 & 0 & 0 \\ 0 & 0 & 0 & 0 & 0 & 0 \\ 0 & 0 & 0 & 0 & 0 & 0 \\ 0 & 0 & 0 & 0 & 0 & 0 \end{bmatrix} \tag{1}$$

where$x_{ASV}, y_{ASV}$ are the position of the ASV, $x_0, y_0$ are the desired holding positions under sway and surge, $C_1, C_2$ are the control force coefficients. During the time-domain calculation, if $C_1, C_2$ are large enough and the time step is sufficiently small, the ship will be limited at the desired location.

The following ASV control force can drive the vessel to keep a constant distance from the ROV when the ROV is approaching its target. When the following ASV recover the ROV, the distance form ROV decreases by the time. The control coefficient will make sure the lateral distance between ASV and ROV is zero when their vertical distance is smaller than 5m. This distance is not a fixed one and based on complicate factors like sea conditions, the facility of the ASV/ROV and winch, the applied control methods and etc. The ASV/ROV designer can choose the suitable values in the sea trail.

$$[C]=\begin{bmatrix} (x_{ROV}-x_{ASV}-x_{distance})*k_{lx}*log_2(z_{ASV}-z_{ROV}) & 0 & 0 & 0 & 0 & 0 \\ 0 & (y_{ROV}-y_{ASV}-y_{distance})*k_{lx}*log_2(z_{ASV}-z_{ROV}) & 0 & 0 & 0 & 0 \\ 0 & 0 & 0 & 0 & 0 & 0 \\ 0 & 0 & 0 & 0 & 0 & 0 \\ 0 & 0 & 0 & 0 & 0 & 0 \\ 0 & 0 & 0 & 0 & 0 & 0 \end{bmatrix} \tag{2}$$

where $x_{ROV}, y_{ROV}$are the position of ROV, $x_{distance}, y_{distance}$are the distance between ASC and ROV.

### *The ROV control*

The control method on the x, y direction offers a gentle way for the ROV's propeller force to increase as a function of its depth to the ASV:

$$F_{lx}=\left(x_{target}-x_{ROV}\right)*k_{lx}*log_2(z_{ASV}-z_{ROV}) \tag{3}$$

$$F_{ly}=\left(y_{target}-y_{ROV}\right)*k_{ly}*log_2(z_{ASV}-z_{ROV}) \tag{4}$$

When $F_{lx}$ and $F_{ly}$ are larger than the maximum thrust of ROV, the maximum thrusts will replace them.

The z-direction force $F_{lz}$ includes a constant component $C_z$ that permits to approach the target plus a Gaussian function around the target allowing the force to increase a lot when approaching the target in

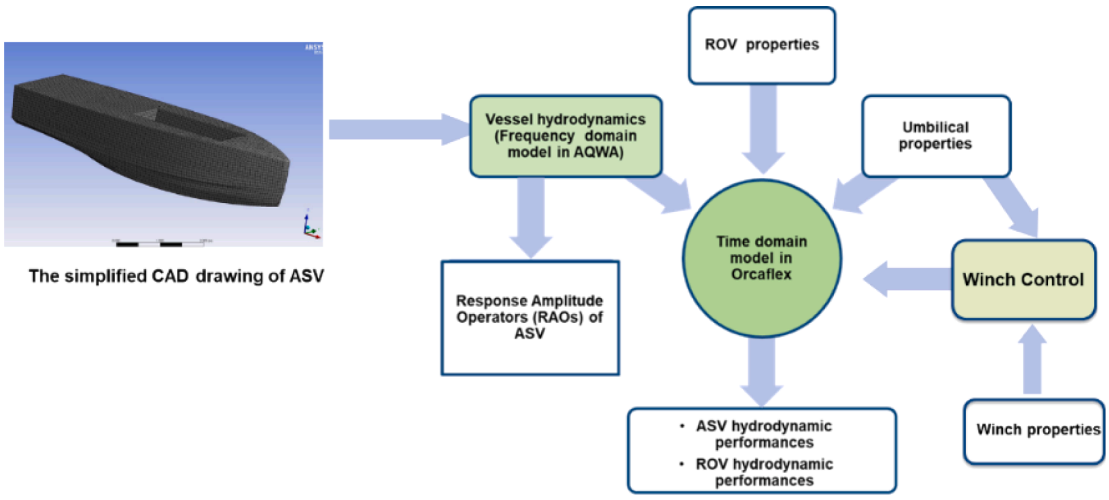


**Fig. 1.** Overview of the numerical model, including a frequency- and a time-domain model.

**Table 1**
Environmental conditions in the model.

| Environment conditions | Value (unit) |
|---|---|
| Significant wave height ($H_s$) | 1 m; 1.5 m; 2 m; 2.5 m; 3 m |
| Peak wave periods ($T_p$) | 4 s |
| Surface tidal current speed ($V_{tidal}$) | 1.2 m/s |
| Water depth ($d$) | 150 m |
| Tidal direction (the ASV/ROV heading angle) ($\theta_{tidal}$) | 0, 30,45, 60 (deg) |

**Table 2**
Properties of the [L3HARRIS. C-Worker 7 2020]ASV L3HARRIS. C-Worker 7 2020.

| Property | Value (unit) |
|---|---|
| Length | 7.2 m |
| Beam | 2.3 m |
| Draft | 0.9 m |
| Weight (without payload) | 4280 kg |
| $C_1$ $C_2$ | 10 kN/m |
| $x_{distance}$ | 0 to 20m |
| $y_{distance}$ | 0 m |

**Table 3**
Properties of the modelled ROV.

| Property | Value (unit) |
|---|---|
| Length | 1 m |
| Width | 0.6 m |
| Height | 0.5 m |
| Weight in the air (with the max payload) | 74 kg |
| Weight in the water | 5 kg |
| Max thrust | Forward = 50 *kgf*<br>*Lateral* = 28 *kgf*<br>*Vertical* = 13 *kgf* |

order to maintain the ROV's depth. Similar to the $F_{lx}$ and $F_{ly}$, $F_{lz}$ will still be limited by the maximum ROV thrust.

*The winch controls*

In this present paper, two different methods are used.

1. The first method, *speed control*, is to maintain the pay-out rate ($v_{out}$) of the umbilical as a constant value, and then to calculate the winch drive force ($F_{drive}$) in the umbilical at any time.

2. The second method, tension *control*, aims to control the tension and to determine the corresponding pay-out rate, respectively.

**Table 4**
Properties of the umbilical and winch.

| Property | Value (unit) |
|---|---|
| Umbilical Diameter | 17 *mm* |
| Umbilical weight in air | 350 *kg/km* |
| Umbilical weight in water | 150 *kg/km* |
| Minimum dynamic bending diameter | 350 *mm* |
| Breaking strength | 18 *kN* |
| Max allow tension | 3 *kN* |
| Winch drum diameter | 0.5 m |
| Winch drum mass | 50 kg |
| Winch speed (speed control) | 0.3 m/s; 0.5 m/s |
| $F_{reuqired}$ | 0.1 kN |
| $c_t$ | 0.5 kN/m |
| $s_{\min}$ | 1 m |
| $s_{\max}$ | 3 m |

For the winch speed control,

$$\mathbf{V}_{\mathbf{t-winch-connect}}(s \quad t) = v_{out} \tag{5}$$

As a result, the $\dot{\mathbf{V}}_{\mathbf{t-winch-connect}}(s \quad t)$ is 0.

The winch drive force is:

$$F_{drive} = T_{tension} + F_{resistance} \tag{6}$$

The resistance of the winch could be presented as:

$$F_{resistance} = d_{db} + c_{out}v_{out} + d_{out}v_{out}^{\ 2} \tag{7}$$

where $d_{db}$ is the winch drive dead-band, $c_{out}$ are the winch drive damping terms for pay-out. $d_{out}$ are the winch drive drag terms for pay-out.

For the tension control method:

$$F_{drive} = F_{target} + F_{resistance} \tag{8}$$

where $F_{target}$ is the target tension on the umbilical.

According to Eq. (6) to (8) and $J_{winch} = M_{winch}R_{winch}^2$

$$v_{out}(s \quad t) = \frac{(F_{target} - T_{tension})}{M_{winch}R_{winch}}t + v_{out}(s_0 \quad 0) \tag{9}$$

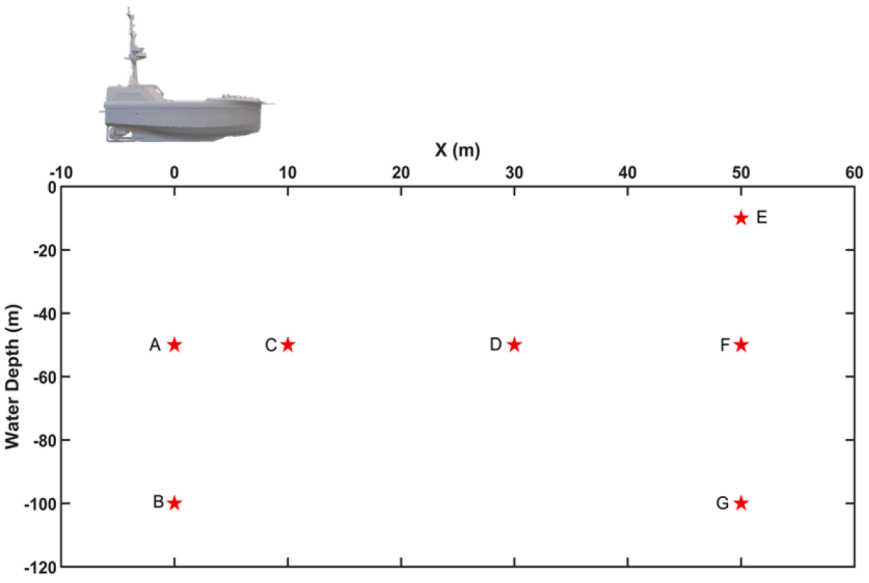


**Fig. 2.** The ROV targets, the ASV initial position is defined as (0,0).

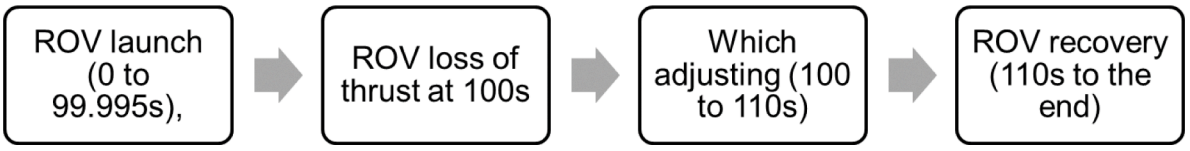


**Fig. 3.** Overview of the ROV malfunction cases.

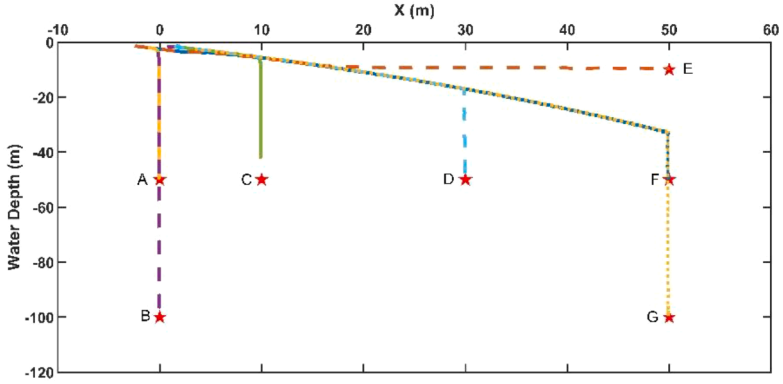


**Fig. 4.** The ROV path in the ROV approaching cases, with a 0.3 m/s winch speed $Hs = 1$ m.

**Table 5**
Duration for ROV reaching target position in each direction, (Hs=1m).

| Target (X, Z) (m) | X time (s) | Z time (s) |
|---|---|---|
| A (0,50) | 0 | 200 |
| B (0,100) | 0 | 480 |
| C (10,50) | 25 | 215 |
| D (30,50) | 101 | 220 |
| E (50,10) | 158 | 52 |
| F (50,50) | 190 | 256 |
| G (50,100) | 200 | 500 |

**Table 6**
The required umbilical length vs Target absolute distance (Hs=1m).

| Target | Umbilical length (m) | Absolute distance (m) | Ratio (-) |
|---|---|---|---|
| A (0,50) | 60 | 50 | 1.2 |
| B (0,100) | 144 | 100 | 1.44 |
| C (10,50) | 62 | 51 | 1.2 |
| D (30,50) | 66 | 58 | 1.13 |
| E (50,10) | 52.5 | 51 | 1.04 |
| F (50,50) | 77 | 70 | 1.1 |
| G (50,100) | 150 | 119 | 1.25 |

In the reality, it is very difficult to maintain a constant tension because the winch control may require an extreme fast speed change, especially under the steep approaching waves. The hydraulic motion compensation system is considered as a partial solution which has been tested and validated in the ROV system (Huster et al., 2009). This study uses a changeable target tension to smooth the fast required speed change of the winch.

When the hydraulic cylinder or ram of the compensation system operates into a safe range (based on the length of the cylinder), the target tension is a constant one:

**Table 7**
Maximum and mean umbilical tension and winch speed (Hs=1m).

| Speed (m/s) | Max (kN) | Mean (kN) |
|---|---|---|
| 0.05 | 0.9 | 0.28 |
| 0.1 | 0.8 | 0.27 |
| 0.15 | 0.76 | 0.27 |
| 0.2 | 0.75 | 0.25 |
| 0.3 | 0.76 | 0.26 |

**Table 8**
Maximum and mean umbilical tension vs tidal current direction (vertical cases).

| Tidal current direction (deg) | Max (kN) | Mean (kN) |
|---|---|---|
| 0 | 0.7 | 0.17 |
| 30 | 0.66 | 0.17 |
| 45 | 0.69 | 0.17 |
| 60 | 0.69 | 0.18 |

$$F_{target} = F_{reuqired} \tag{10}$$

When the relative motion between the ASV and ROV exceeds the capacity of the compensation system:

If the motion amplitude of the cylinder/rum ($s_c$) > maximum limitation of the safe range ($s_{\max}$):

$$F_{target} = F_{reuqired} + c_t(s_c - s_{\max}) \tag{11}$$

If $s_c < s_{\min}$,

$$F_{target} = F_{reuqired} + c_t(s_{\min} - s_c) \tag{12}$$

where the $c_t$ is the control coefficient in the tension control.

In this study, hydrodynamic drag forces of the umbilical are represented by the drag term in Morison's equation (Aamo and Fossen, 2000). The drag forces applied to a line are calculated using the cross-flow principle. That is, the fluid velocity relative to the line is split into its components $\mathbf{v_n}$ and $\mathbf{v_z}$normal and parallel to the line axis. The drag force normal to the line axis is then determined by$\mathbf{v_n}$ and its x- and y-components $v_x$and $v_y$; the drag force parallel to the line axis is determined by vz. The drag force formulae use drag coefficients, $C_{Dx}$, $C_{Dy}$ and $C_{Dz}$, and the drag areas appropriate to each direction.

**Table 9**
Umbilical parameters and ROV target time with ASV following (Hs=1m).

| Target | X time (s) | Z time (s) | Umbilical length (m) | Tension Max (kN) | Tension Mean (kN) |
|---|---|---|---|---|---|
| F (50,50) stationary ASV | 190 | 256 | 77 | 0.77 | 0.26 |
| *F 5m* | 86 | 210 | 63 | 0.58 | 0.15 |
| *F 10m* | 100 | 213 | 64 | 0.7 | 0.17 |
| *F 15m* | 112 | 210 | 64 | 0.71 | 0.18 |
| *F 20m* | 124 | 210 | 64 | 0.72 | 0.19 |

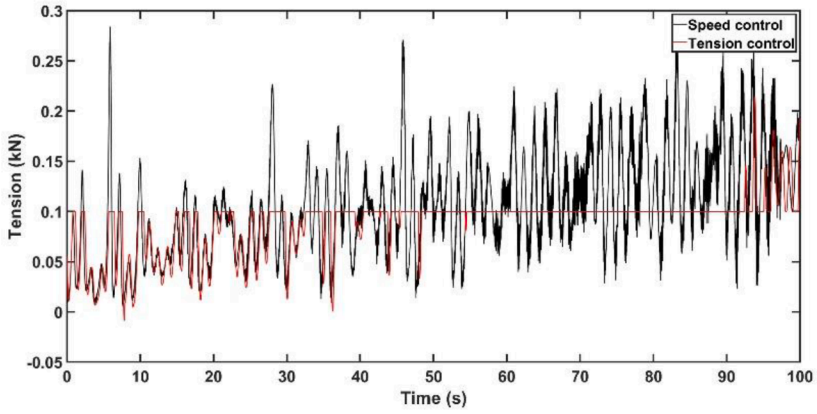


(a)

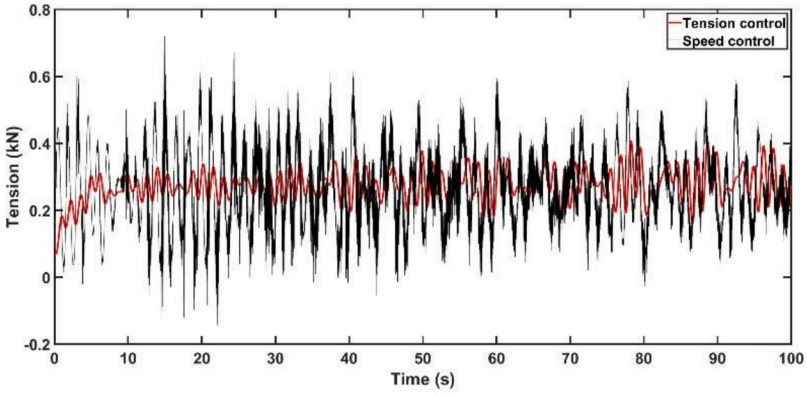


(b)

**Fig. 5.** The umbilical tension under two control methods, with a 0.3 m/s in speed control, $Hs$ = 1 m (a) Vertical case Target A; (b) Vertical/Lateral case, Target F.

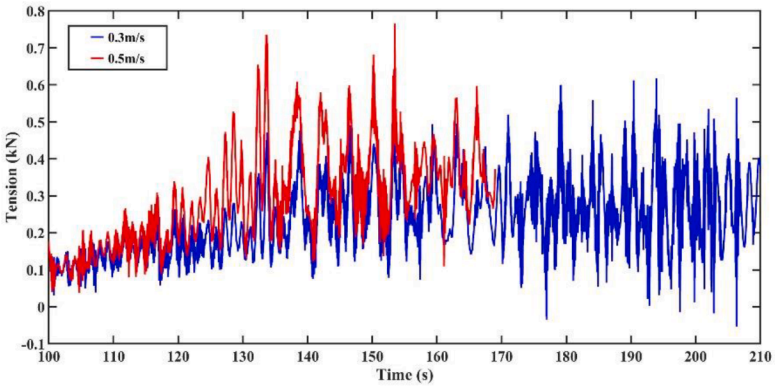


(a)

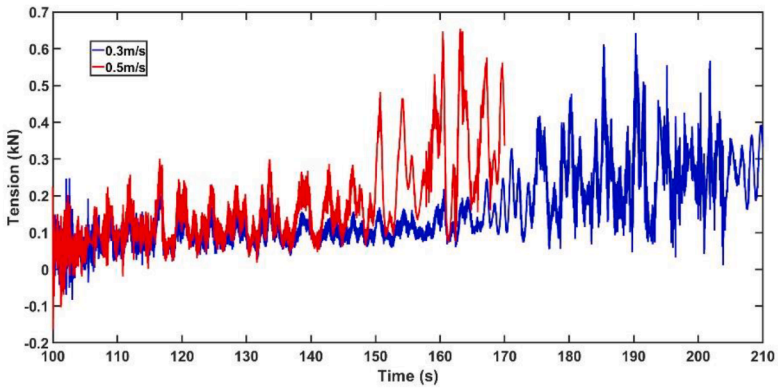


(b)

**Fig. 6.** Umbilical tension for different winch speeds during adjusting and recovery stage, stationary ASV: (a) Vertical cases (b) Vertical/lateral cases.

$$f_{dx} = \frac{1}{2} p\rho d_n l C_{Dx} |\mathbf{v_n}| \tag{13}$$

$$f_{dy} = \frac{1}{2} p\rho d_n l C_{Dy} v_y |\mathbf{v_n}| \tag{14}$$

$$f_{dz} = \frac{1}{2} p\rho \pi d_a l C_{Dz} v_z |v_z| \tag{15}$$

Where $p$is proportion wet, $\rho$is the water density, $d_n$ the normal drag diameter, $l$is the length of line represented by the node. $d_a$ is the axis drag diameter.

## Numerical modelling

### *Model illustration*

An overview of the modelling scope is provided in Fig. 1. The hydrodynamic coefficients of the ASV are solved in the frequency domain. The control forces and other nonlinear forces are defined and solved in the time domain. The control methods of the ASV, ROV and winch system are programmed by the python codes. The numerical tool is the commercial code Orcaflex, which is based on the above method. It is one of the leading packages for the dynamic analysis of offshore marine systems (Arramounet et al., 2019, Thomsen et al., 2017, Paduano et al., 2020). OrcaFlex has been widely used across the academic and engineering community. The details of this model were illustrated in (Zhao et al., 2020, Zhao et al., 2021).

### *Input conditions*

The input conditions involve environment conditions and the parameters of ASV, ROV and the winch system.

### *Environment conditions*

The selected environment conditions are based on the weather window of the potential sea trial site (FaBTest) (Ashton et al., 2014). The waves are defined by the JONSWAP spectrum (Hasselmann et al., 1973) and the tidal current speed distribution along the water depth is calculated the power law (Hagerman et al., 2006). The details are listed in Table 1.

### *ASV/ROV/Winch parameters*

The parameters of the ASV/ROV/Winch are listed in the below tables.

Table 2,3 Table 4Fig. 11

### *Cases*

This paper explores the winch/umbilical performance via a range of cases, including different targets and control methods.

### *ROV targets*

A total of eight targets with different water depths and distances from the ASV are selected to evaluate the umbilical tension performance, see Fig. 2. Targets A and B lie vertically below the ASV with 50 m

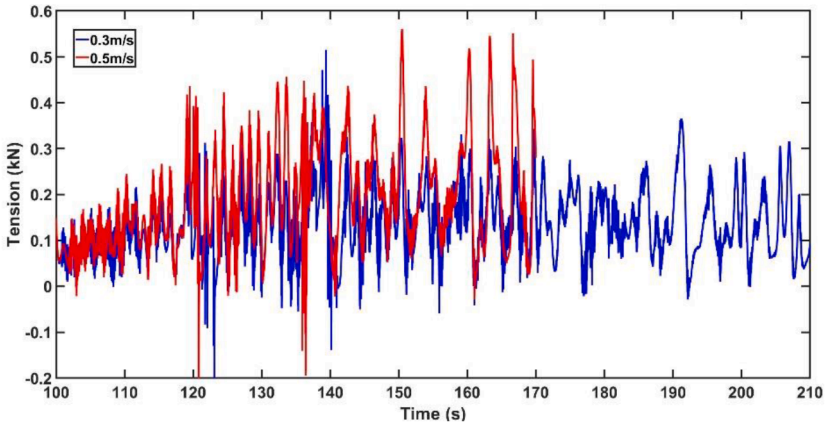


(a)

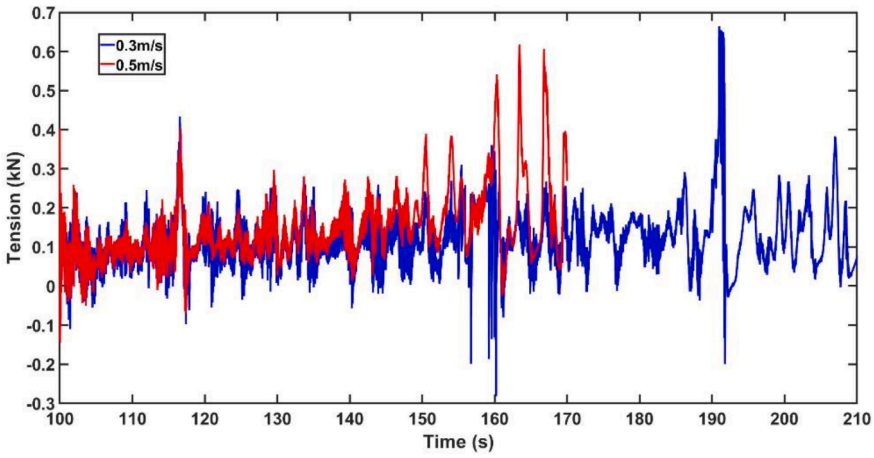


(c) (d)

**Fig. 7.** Umbilical tension for different winch speeds during adjusting and recovery stage, following ASV: (a) Vertical cases. (b)Vertical/lateral cases.

**Table 10**
Comparison of umbilical tension parameters for ROV ALS recovery, (Hs=1m).

| | Follow max (kN) | Stationary max (kN) | Difference | Follow mean (kN) | Stationary mean (kN) | Difference |
|---|---|---|---|---|---|---|
| Vertical, adjusting stage, 0.5m/s | 0.2 | 0.21 | -5% | 0.09 | 0.13 | -30% |
| Vertical, Recovery stage, 0.5m/s | 0.56 | 0.77 | -27% | 0.2 | 0.32 | -37% |
| Vertical, adjusting stage, 0.3m/s | 0.19 | 0.2 | -5% | 0.08 | 0.12 | -33% |
| Vertical, Recovery stage, 0.3m/s | 0.51 | 0.62 | -18% | 0.14 | 0.25 | -44% |
| Vertical/lateral, adjusting stage, 0.5m/s | 0.21 | 0.22 | -4% | 0.07 | 0.08 | -12.5% |
| Vertical/lateral, Recovery stage, 0.5m/s | 0.6 | 0.65 | -7% | 0.18 | 0.2 | -10% |
| Vertical/lateral, adjusting stage, 0.3m/s | 0.22 | 0.24 | -8% | 0.064 | 0.07 | -8.5% |
| Vertical/lateral, Recovery stage, 0.3m/s | 0.61 | 0.64 | -5% | 0.14 | 0.16 | -12.5% |

and100 m depth, respectively. Targets E, F and G with are located at 10 m, 50 m, and 100 m depth, with a horizontal distance (x-direction) from ASV of 50 m. Targets A, C, D and F share the same 50 m water depth with 0 m, 10 m, 30 m, and 50 m distance from the ASV. These targets can be classified into vertical targets (A and B) and vertical/horizontal targets (C to G).

*ROV approaching cases*

The ROV approaching cases aim to evaluate the umbilical tension and length when the ROV is approaching all targets. The ASV applies both non-following/following control. The $x_{distance}$ in the ROV following control is set to 5m, 10m, 15m and 20m offset respectively. The effects caused by different winch speeds and tidal current direction are also considered.

*ROV accidental limit state cases*

The accidental limit state (ALS) is considered to be the ROV malfunctioning, i.e. complete loss of thrust, to explore the umbilical performance when an unexpected malfunction of ROV suddenly occurs during the launch stage. The ROV loses all thrusts at this stage, and the winch hauls in the umbilical within 10 s. The stage that the winch adjusts its speed to haul in the ROV is denoted as adjusting stage. In the

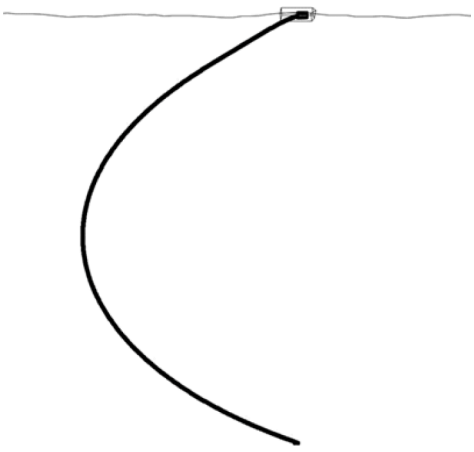

**Fig. 8.** Umbilical shape in the Target B case, with the bending radius 100 m.

recovery stage, the winch recovers the ROV with its maximum speed (0.5 m/s). The workflow of the ROV ALS case is shown in Fig. 3

## Results

This section presents results of all ROV target profiles for the different ASV control strategies (stationary and following the ROV) and the ROV ALS malfunction cases.

*ROV target profiles*

*Stationary ASV*

Fig. 4 shows the paths of the ROV during the target approaching stages, with a 0.3 m/s winch speed. In the modelled conditions, the ROV was able to reach all targets. The results show that the ROV thrust is sufficient for the selected range of targets. The thrust could independently maintain the ROV position on both x- and y- direction (such as E and F). However, the ROV velocity varies for the different targets (Table 5). For example, the ROV takes longer to reach Target G depth, compared to the same depth of target B case.

The required umbilical length to reach a given target position is a critical factor during the sea trial because it influences the ASV payload, accordingly. Table 6 presents the required length for different ROV. The last column calculates the umbilical length ratio:

$R$ = umbilical length / absolute distance. This is a useful engineering factor to estimate the required umbilical length for a given ROV target. The results suggest that a ratio of $R = 1.5$ is sufficient in all cases. Thus, the umbilical length should be at least 1.5 times the planned absolute distance between the ROV and the stationary ASV.

Table 7 shows the umbilical tension when the ROV is approaching the Target F (50,50) with different winch speeds. A speed threshold that decouples the winch speed and the umbilical tension can be observed. For this ASV/ROV system, the winch speed threshold is 0.15 m/s. Results in Table 8 show that the umbilical tension is not sensitive to the tidal current direction. Both mean and max tension on the umbilical are similar for the range of tidal current directions.

The time series of umbilical tension under different winch control

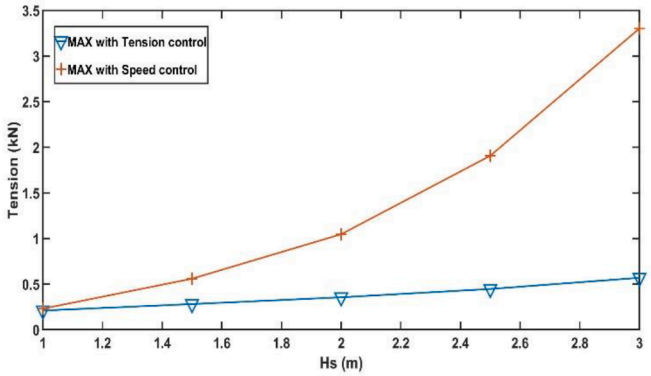


(a)

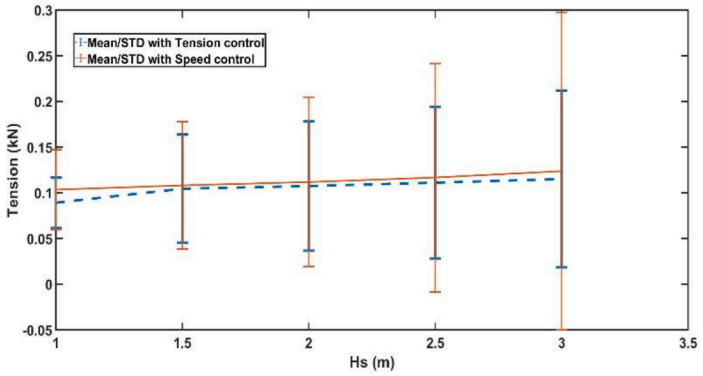


(b)

**Fig. 9.** Umbilical tension under winch speed control and tension control, (a) Max tension; (b) STD and Mean tension.

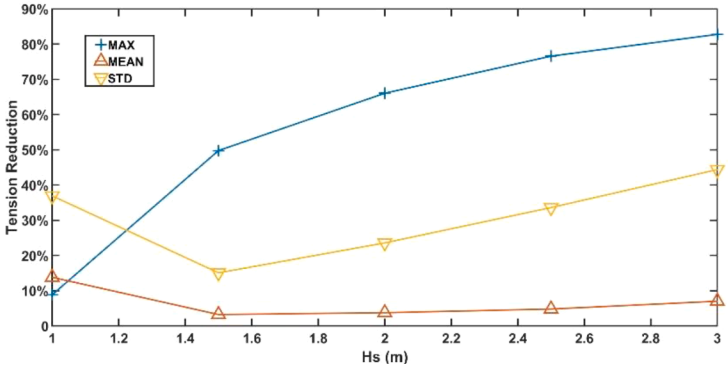


**Fig. 10.** Umbilical tension reduction in the tension control, compared the speed control.

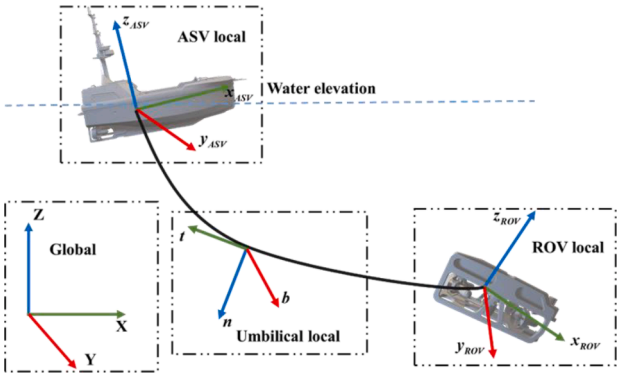


**Fig. 11.** The coordinates of an ASV/ROV system.

methods are shown in Fig. 5. It can be observed that the umbilical experiences less and much more stable tension for the tension controlled (the initial target tension is 0.1 kN) winch for both cases.

*Following ASV*

This section presents the results for the second ASV control strategy, where it is following the ROV at given horizontal offsets. Table 9 compares the results of target *F* (50, 50) with following/non-following ASV. The following ASV reduces both max and mean tensions on the umbilical. In addition, for this ASV strategy, the ROV also reaches the target quicker and uses a shorter required umbilical length.

*ROV malfunction cases*

For the ROV ALS malfunction cases, two winch recovery speeds are modelled, 0.5 m/s and 0.3 m/s. Fig. 6 presents the time series of umbilical tension a stationary ASV. The tension amplitude increases when the winch begins to haul the ROV in for the vertical cases (see the tension in Fig. 6 However, the tension amplitude will first decrease and then increase in vertical/lateral cases [see Fig. 6 (b)]. In all cases, the peak tension appears when the ROV is close to the ASV (absolute distance less than 10 m). Compression of the umbilical is also observed during the adjusting and recovery stages, which could be prevented by a faster haul in speed. The umbilical tension with a following ASV is presented in Fig. 7. The changing trends of tension are in line with that in stationary ASV cases, but the changing rate is much lower, which results in smaller tension amplitude.

Table 10 compares the umbilical tension with a following/stationary ASV, respectively. The results show that the strategy where the ASV follows the ROV decreases the umbilical tension in the adjusting and recovery stage. The tension reduction is more significant in the recovery stage. It is also observed that the following ASV reduces more tension in the vertical cases (up to 44% in vertical cases and only 12.5% in vertical/lateral cases).

## Discussion

This study uses a numerical approaching to explore the winch performance and the resultant umbilical parameters of an ASV/ROV system in a range of operating scenarios. The results in Section 4 include the umbilical tension and length performance in both ROV launching and recovery situations. The following/ stationary ASVs are also considered.

In the ROV launching cases, the ROV could successfully reach all targets. For the winch speed effect, a relatively slower winch speed will lead a higher tension. For the ASV/ROV system in this paper, the threshold which could decouple the umbilical tension and the winch speed is 0.15 m/s. The umbilical length results suggest that the required length can be calculated as 1.5 times of the absolute distance between the target and ASV. This deployment can handle the sudden relative motion between ASV and ROV caused by the steep approaching waves. The maximum bending of umbilical occurs in the Target B (Fig. 8), but this bending radius is still much larger than the minimum dynamic bending radius (100 m and 0.175 m).

Compared to the winch speed control, the tension control allows the ASV/ROV system to operate in a harsher wave environment. The tension control can reduce all the mean, max, and Standard Deviation (STD) of tension amplitudes. It is also observed that the tension control mainly limits the max tension amplitude and smooths the tension change. Its effects on the mean tension are not significant (Fig. 9 and Fig. 10). As a consequence, the winch designer should balance the advantages brought by the tension control and the cost, as well as the ASV payload, based on the sea conditions and the task requirements. The tension control is not very effective for normal wave conditions (e.g. Hs = 1 m and 1.5 m), and it needs an additional hydraulic (motion compensation) system to stabilise the winch speed, which will occupy more space and payload of the ASV.

The following ASV strategy can reduce umbilical tension in both ROV launching and malfunction cases. The following ASV strategy also has the advantage that it reduces the absolute distance between ASV and ROV, allowing more lazy-wave umbilical to buffer the tension, whilst also reducing the required umbilical length. The weak point of the following ASV is that it will compress the umbilical, leading a negative tension. This is caused by the speed of the distance (ASV and ROV) decrease is faster than the winch haul-in speed. As a result, a faster haul-in speed can reduce the times that the umbilical compression occurs. Another disadvantage is that the ROV is typically very agile with a large degree of motion. Thus if the ASV control is linked to the ROV position, as modelled in this paper, it necessitates a suitable system to i) track the ROV in relation to the ASV (Conte et al., 2016), typically realised through an acoustic beacon, and ii) integrated ASV control to react to ROV position changes (Cho et al., 2020). Aguiar et al. (2009) also gave a very comprehensive review to show the challenges existing in the

ASV/ROV integrated control.

Results in Table 10 showed that the tension reduction caused by the following ASV is more effective in vertical cases. It is believed that ASV and ROV already has a horizontal distance which can buffer the umbilical tension. The following ASV just reduce/maintain this distance.

As shown in Table 7, it is useful to determine a winch speed threshold parameter that allows to limit, i.e. decouple, the umbilical tension from the winch speed. Both the maximum and mean tension trend to be constant (0.75 kN for max and 0.26 kN for mean) if the winch speed exceeds 0.15 m/s. The using the presented methods, a suitable winch speed threshold can be determined for different system configurations.

The presented model can be generally applied. The numerical model is built based on the potential flow theory. Thus, the additional hydrodynamic viscous damping should be quantified through experimental decay tests in the future. The results of this paper aim to guide a future ASV/ROV sea trial. Therefore, the numerical model will be validated and calibrated by the sea trial data. Additionally, the latest version Orcaflex cannot consider the Strouhal number and feeding line (known as the umbilical in the study) at the same time. Thus, the Strouhal number is not taken into consideration at the current stage. As a result, an experiment test will be conducted to quantify both exact Strouhal number and its effects in our future research. Finally, the control method of the ROV and ASV should be optimised based on their facilities, when sufficient data from sea trials, are obtained.

## Conclusion

The paper has systematically explored the winch design and performance in an ASV/ROV system. The stationary/following ASV strategies, different ROV scenarios and the winch with a motion compensation system were modelled by analytical and numerical means. The main findings of this study are:

a) Compared to the stationary ASV, the following ASV can reduce and smooth the tension on the umbilical during both ROV launch and recovery stages.
b) The following ASV will produce compression on the umbilical in the ROV recovery stage, which should be mitigated by increasing the winch haul-in speed.
c) For the ASV/ROV system in this study, the required umbilical length can be estimated as 1.5 times of the absolute distance from the ASV to the ROV target.
d) A threshold exists to decouple the winch speed and the umbilical tension, for the ASV/ROV here, the value is 0.15 m/s. For other systems this threshold will increase with larger ROV thrusts.
e) Compared to the speed control, the tension control mainly decreases the maximum tension. The tension reduction caused by winch control is not significant for cases where the significant wave height $Hs < 1$ m.

## Declaration of Competing Interest

**The authors have no conflict of interest to declare.**

*Credit Author Statement*

**Philipp R. Thies**: Conceptualization, Methodology, Funding acquisition, project administration, Writing – Review & Editing. **Chenyu Zhao**: Writing – Original Draft, Data Curation, Investigation, Software, visualization. **Lars Johanning**: Writing: Reviewing and Editing, Supervision.

*Acknowledgements*

This study has received funding through the project “Autonomous Robotic Intervention System For Extreme Maritime Environments (ARISE) Stage 2”, as part of the Industry Strategy Challenge Fund (ISFC) funded by Innovate U.K. (UKRI), Project Reference: 104831. The support through Orcina through the provision of their Orcaflex software s also kindly acknowledged. The second author would also like to acknowledge funding through the EPSRC Supergen ORE Hub [EP/S000747/1].

## Supplementary materials

Supplementary material associated with this article can be found, in the online version, at doi:10.1016/j.apor.2021.102827.

## References

DeCastro, M, Salvador, S, Gómez-Gesteira, M, Costoya, X, Carvalho, D, Sanz-Larruga, F, et al., 2019. Europe, China and the United States: three different approaches to the development of offshore wind energy. Renew. Sustain. Energy Rev. 109, 55–70.
Lian, J, Cai, O, Dong, X, Jiang, Q, Zhao, Y., 2019. Health monitoring and safety evaluation of the offshore wind turbine structure: a review and discussion of future development. Sustainability 11, 494.
Chung, H-M, Maharjan, S, Zhang, Y, Eliassen, F, Strunz, K., 2020. Placement and Routing Optimization for Automated Inspection with UAVs: A Study in Offshore Wind Farm. arXiv preprint arXiv, 200608326.
Jin, R, Hou, P, Yang, G, Qi, Y, Chen, C, Chen, Z., 2019. Cable routing optimization for offshore wind power plants via wind scenarios considering power loss cost model. Appl. Energy 254, 113719.
organisation Ghas. 2019 incident data report. 2020.
Hill, C., 2019. Robotics and autonomous systems. Econ. Opport.
Capocci, R, Dooly, G, Omerdić, E, Coleman, J, Newe, T, Toal, D., 2017. Inspection-class remotely operated vehicles—a review. J. Marine Sci. Eng. 5, 13.
Kyo, M, Hiyazaki, E, Tsukioka, S, Ochi, H, Amitani, Y, Tsuchiya, T, et al., 1995. The sea trial of" KAIKO", the full ocean depth research ROV. In: , pp. 1991–1996.
Mikagawa, T, Fukui, T., 1999. 10,000-meter class deep sea ROV" KAIKO" And underwater operations. The ninth international offshore and polar engineering conference. In: International Society of Offshore and Polar Engineers.
Ishibashi, S, Yoshida, H, Watanabe, Y, Osawa, H, Tahara, J, Miyazaki, T, et al., 2007. Development of a sediment sampling system for the deepest ocean and its sea trial result. In: The Seventeenth International Offshore and Polar Engineering Conference: International Society of Offshore and Polar Engineers.
Nakajoh, H, Murashima, T, Sugimoto, F., 2018. Development of full depth fiber optic cable ROV (UROV11K) system. In: OCEANS 2018 MTS/IEEE Charleston: IEEE, pp. 1–8.
Bruno, F, Muzzupappa, M, Lagudi, A, Gallo, A, Spadafora, F, Ritacco, G, et al., 2015. A ROV for Supporting the Planned Maintenance in Underwater Archaeological Sites. Oceans 2015-Genova. IEEE, pp. 1–7.
Sivčev, S, Omerdić, E, Dooly, G, Coleman, J, Toal, D., 2017. Towards inspection of marine energy devices using rovs: floating wind turbine motion replication. Iberian Robotics Conference. Springer, pp. 196–211.
Rush, B, Joslin, J, Stewart, A, Polagye, B., 2014. Development of an adaptable monitoring package for marine renewable energy projects part I. Concept. Design Operation.
Joslin, J, Rush, B, Stewart, A, Polagye, B., 2014. Development of an adaptable monitoring package for marine renewable energy projects part II. Hydrodyn. Perform.
Sun Y-s, Wan, L, Gan, Y, Wang, J-g, Jiang, C-m., 2012. Design of motion control of dam safety inspection underwater vehicle. J. Central South University 19, 1522–1529.
Cruz, NA, Matos, AC, Almeida, RM, Ferreira, BM, Abreu, N., 2011. TriMARES-a hybrid AUV/ROV for dam inspection. In: OCEANS'11 MTS/IEEE KONA: IEEE, pp. 1–7.
Chen, H-H, Chuang, W-N, Wang, C-C., 2015. Vision-based line detection for underwater inspection of breakwater construction using an ROV. Ocean Eng. 109, 20–33.
Yu, F, Li, Q, Wang, Y, Chen, Y., 2021. Optimization of tool orientation for improving the cleaning efficiency of offshore jacket-cleaning systems. Appl. Ocean Res. 112, 102687.
Negahdaripour, S, Firoozfam, P., 2006. An ROV stereovision system for ship-hull inspection. IEEE J. Oceanic Eng. 31, 551–564.
Matsuda, T, Takizawa, R, Sakamaki, T, Maki, T., 2020. Landing method of autonomous underwater vehicles for seafloor surveying. Appl. Ocean Res. 101, 102221.
Chen, G, Yang, X, Zhang, X, Hu, H., 2021. Water hydraulic soft actuators for underwater autonomous robotic systems. Appl. Ocean Res. 109, 102551.
Zhao C, Thies P, Johanning L, Tobin S. Modelling and assessment of ROV capacity within an autonomous offshore intervention system. 2020.
Gray, A, Schwartz, E., 2016. Anglerfish: an ASV controlled ROV. In: 29th Florida Conference on Recent Advances in Robotics (FCRAR). Miami, FL.
Conte, G, Scaradozzi, D, Mannocchi, D, Ciuccoli, N., 2017. Field test of an integrated ASV/ROV platform. In: The 27th International Ocean and Polar Engineering Conference: International Society of Offshore and Polar Engineers.
Conte, G, Scaradozzi, D, Mannocchi, D, Raspa, P, Panebianco, L, Screpanti, L., 2016. Experimental testing of a cooperative ASV-ROV multi-agent system. IFAC-PapersOnLine 49, 347–354.
Sarda, EI, Dhanak, MR., 2016. A USV-Based automated launch and recovery system for AUVs. IEEE J. Oceanic Eng. 42, 37–55.

Sivčev, S, Coleman, J, Omerdić, E, Dooly, G, Toal, D., 2018. Underwater manipulators: a review. Ocean Eng. 163, 431–450.
Trslic, P, Rossi, M, Robinson, L, O'Donnel, CW, Weir, A, Coleman, J, et al., 2020. Vision based autonomous docking for work class ROVs. Ocean Eng. 196, 106840.
Nordås, S, Andersen, T, Ebbesen, M., 2017. The potential of a digital hydraulic winch drive system. In: Proceedings of the Ninth Workshop on Digital Fluid Power, pp. 7–8. Sep.
Pardo, ML, Carral Couce, L, Castro-Santos, L, Carral Couce, JC, 2017. A review of the drive options for offshore anchor handling winches. Brodogradnja 68, 119–134.
Fossen, TI., 1999. Guidance and Control of Ocean Vehicles. University of Trondheim, Norway, Printed by John Wiley & Sons, Chichester, England. ISBN: 0 471 94113 1, Doctors Thesis.
Feng, Z, Allen, R., 2004. Evaluation of the effects of the communication cable on the dynamics of an underwater flight vehicle. Ocean Eng. 31, 1019–1035.
Huster, A, Bergstrom, H, Gosior, J, White, D., 2009. Design and operational Performance of a Standalone Passive Heave Compensation System for a Work Class ROV. OCEANS 2009. IEEE, pp. 1–8.
Aamo, OM, Fossen, TI., 2000. Finite element modelling of mooring lines. Math. Comput. Simul 53, 415–422.
Arramounet, V, de Winter, C, Maljaars, N, Girardin, S, Robic, H., 2019. Development of coupling module between BHawC aeroelastic software and OrcaFlex for coupled dynamic analysis of floating wind turbines. Journal of Physics: Conference Series. IOP Publishing, 012007.
Thomsen, JB, Ferri, F, Kofoed, JP., 2017. Validation of a tool for the initial dynamic design of Mooring systems for large floating wave energy converters. J. Marine Sci. Eng. 5, 45.
Paduano, B, Giorgi, G, Gomes, RP, Pasta, E, Henriques, JC, Gato, L, et al., 2020. Experimental validation and comparison of numerical models for the mooring system of a floating wave energy converter. J. Marine Sci. Eng. 8, 565.
Zhao, C, Thies, P, Lars, J, Cowles, J., 2021. ROV launch and recovery from an unmanned autonomous surface vessel–Hydrodynamic modelling and system integration. Ocean Eng. 232, 109019.
Ashton I, Blundy R, Harnois V, Morvan A, Johanning L. Data collection, analysis and provision for the FaBTest site. 2014.
Hasselmann, K, Barnett, TP, Bouws, E, Carlson, H, Cartwright, DE, Enke, K, et al., 1973. Measurements of wind-wave growth and swell decay during the Joint North Sea Wave Project (JONSWAP). Ergänzungsheft 8-12.
Hagerman, G, Polagye, B, Bedard, R, Previsic, M., 2006. Methodology for estimating tidal current energy resources and power production by tidal in-stream energy conversion (TISEC) devices. In: EPRI North American Tidal in Stream Power Feasibility Demonstration Project, 1.
L3HARRIS. C-Worker 7 https://www.asvglobal.com/product/c-worker-7/. 2020.
Conte, G, De Capua, G, Scaradozzi, D., 2016. Designing the NGC system of a small ASV for tracking underwater targets. Rob. Autom. Syst. 76, 46–57.
Cho, H, Jeong, S-K, Ji, D-H, Tran, N-H, Choi, H-S, 2020. Study on control system of integrated unmanned surface vehicle and underwater vehicle. Sensors 20, 2633.
Aguiar AP, Almeida J, Bayat M, Cardeira B, Cunha R, Häusler A, et al. Cooperative control of multiple marine vehicles theoretical challenges and practical issues. IFAC Proceedings Volumes. 2009;42:412-7.